This article has been accepted for publication in IEEE Control Systems Letters. This is the author's version which has not been fully edited and content may change prior to final publication. Citation information: DOI 10.1109/LCSYS.2021.3114143

String Stability in Microgrids using Frequency Controlled Inverter Chains

Guilherme F. Silva, *Student Member, IEEE*, Alejandro Donaire, *Member, IEEE*, Maria M. Seron, Aaron McFadyen, *Member, IEEE*, and Jason Ford

***Abstract*— In this paper we identify, and propose a solution for, the string stability problem that may arise in frequency droop control schemes for a type of inverter-based microgrid. We consider a previously proposed frequency droop control with secondary control loop and we investigate the effect on the performance due to an increase in the number of inverters connected to the microgrid. To mitigate the observed performance deterioration, we propose a new controller that guarantees string stability of the inverter-based microgrid and show its performance via simulations.**

***Index Terms*— Agents-based systems, distributed control, smart grid.**

I. Introduction

THE decentralisation of energy generation introduced the concept of microgrids, that is, energy networks that can operate disconnected from the main grid. Most decentralised generators operate in DC, and power inverters are used to convert from DC to AC voltage. Inverters are key elements of the microgrids since they can be controlled to ensure a high network performance by synchronising frequencies/voltages and sharing active/reactive power between inverters.

The hierarchical control of inverter-based microgrids is done in three levels: primary, secondary, and tertiary levels [1]. The control design for each level considers the frequency control and the voltage control. The primary level is performed by a droop controller, which is responsible for active/reactive power sharing, and synchronisation of inverters frequencies/voltages. The secondary level, usually an integral-type controller, is responsible for compensating frequency/voltage steady-state errors while preserving active/reactive power sharing. The third level typically manages the power flow between the microgrid and the main grid, when the microgrid is in grid-connected mode.

In recent years there has been considerable research interest in studying theoretical properties of the frequency control and voltage control of inverter-based microgrids [2], [3], such as frequency and voltage synchronisation of the inverters [4], active and reactive power sharing so that the inverters operate close to their power ratings, boundedness of trajectories [5], frequency and voltage regulation [6]–[8]. A common strategy in the treatment of these problems is to separate the analysis into frequency/active-power (ω-P) control and voltage/reactive power control (V-Q) [5], [9].

In this work, we focus our attention on ω-P control assuming the voltages of the inverters are constant (see [10] for a discussion on this "decoupling approximation"). The ω-P droop controller with secondary layer is always stable for any gain choice and preserves power sharing while eliminating frequency steady-state errors [11]. However, previous research in this area has not considered the problem of *string instability*. That is the amplification of disturbances, such as active power increase due to load changes, from inverter to inverter, and performance degradation when the number of inverters in the microgrid increases. We show that string instability behaviour might arise for some configurations, system characteristics and model parameters. We then propose a control design that guarantees string stability while maintaining a good transient performance and power sharing.

Our main contributions are then: *i)* the identification of string instability behaviour that can arise in inverter-based microgrids, and *ii)* to propose a control structure for which we can select controller gains that ensure string stability for a "chain" of inverters.

The rest of the paper is organised as follows. In Section 2, we present the network dynamics and the problem formulation. The control objectives, the sufficient conditions for disturbance string stability (DSS), and control design are presented in Section 3. We present simulation results in Section 4 and conclusions in Section 5.

II. Network model

In this section, we present the network model of an inverter "chain" with the standard primary frequency droop control, which regulates local frequency, and the secondary control loop, which compensates for regulation errors and synchronises the frequency to the desired reference value. We also discuss the potential performance deterioration of the network due to the increase of the number of inverters, a phenomenon known as string instability in the literature related to automated car platoons.

We consider a network of voltage source inverters interconnected via purely inductive lines (justified as the inverter output impedances are controlled to dominate over the network

G. F. Silva, A. McFadyen and J. Ford are with the School of Electrical Engineering and Robotics, Queensland University of Technology, 2 Geroge St, 4000, QLD, Australia. (g.froessilva, aaron.mcfadyen, j2.ford)@qut.edu.au

A. Donaire and M. Seron are with the College of Engineering, Science and Environment, The University of Newcastle, University Drive, 2308, NSW, Australia. (alejandro.donaire, maria.seron)@newcastle.edu.au

This article has been accepted for publication in IEEE Control Systems Letters. This is the author's version which has not been fully edited and content may change prior to final publication. Citation information: DOI 10.1109/LCSYS.2021.3114143

impedances, see [10], [12] for further discussions on this assumption), and define the set $\mathcal{N} \triangleq \{1, 2, \ldots, n\}$, where $n \in \mathbb{N}$ is the total number of inverters. Nevertheless, note that the approach proposed in our paper can be similarly applied to non-inductive lines. The inverters are interconnected in a radial network topology, that is a "chain" of inverters, where each node $i \in \mathcal{N}$ is connected to 2 neighbouring nodes $j \in \mathcal{N}_i$ as follows: $\mathcal{N}_1 = \{2\}$, $\mathcal{N}_i = \{i-1, i+1\}$, for $i = 2, \ldots, n-1$, and $\mathcal{N}_n = \{n-1\}$.

We denote the voltage phase angle by $\delta_i \in \mathbb{R}$ and magnitude by $V_i \in \mathbb{R}^+$, at each node $i = 1, \ldots, n$, and the electrical frequency is given by

$$\dot{\delta}_i = \omega_i \in \mathbb{R}. \tag{1}$$

The total active power flow P_i, at each node, is (see [9])

$$\begin{aligned} P_i &= P_{L,i} + P_{I,i} \\ &= P_{L,i} + \sum_{j \in \mathcal{N}_i} |B_{ij}| V_i V_j \sin(\delta_i - \delta_j), \end{aligned} \tag{2}$$

where $P_{L,i}$ is the active power demand of the load connected to the ith inverter node and $P_{I,i}$ is the injected active power in inverter i. The susceptance of the line between i and j nodes is $B_{ij} < 0$, and we define $B_{ii} = \sum_{j \in \mathcal{N}_i} B_{ij} + \hat{B}_{ii}$, where $\hat{B}_{ii} < 0$ is the shunt (load) susceptance at node i. Also, as in [10], [12] we consider V_i constant and define

$$\alpha_{ij} = |B_{ij}| V_i V_j, \quad i, j = 1, \ldots, n, \quad i \neq j. \tag{3}$$

A. Primary and secondary control

We now formulate the primary and secondary control to derive the closed-loop system dynamics.

1) Frequency Droop Control: The ω-P droop control for inductive lines regulates the local frequency using a term proportional to the active power balance as follows [1]

$$\omega_i = \omega^* - \eta_i (P_i^m - P_i^*) \tag{4}$$

where ω^* and P_i^* are the frequency and power set-points, respectively, and P_i^m is the measured active power obtained from a first-order filter applied to P_i in (2), that is

$$\tau_i \dot{P}_i^m = -P_i^m + P_i \tag{5}$$

where $\tau_i > 0$ is the time constant of the filter.

Combining (4) and (5), we obtain the primary control loop dynamics, which has the form

$$\dot{\delta}_i = \omega_i, \tag{6}$$

$$\dot{\omega}_i = -\tau_i^{-1} \left(\omega_i - \omega^* - \eta_i (P_i - P_i^*) \right). \tag{7}$$

2) Secondary Control Loop: As the frequency droop control provides only proportional control action, it does not ensure zero steady-state regulation error and the synchronised frequency might not achieve the desired value. Thus, it is common to add integral action through a secondary control loop. We consider the consensus algorithm described in [11]

$$k_i \dot{\xi}_i = -(\omega_i - \omega^*) - \sum_{j=1}^{n} g_{ij} (\xi_i - \xi_j) \tag{8}$$

where ξ_i is the state of the secondary controller, the constants k_i are the secondary control gains, and $g_{ij} = g_{ji}$ are the entries of the weighted adjacency matrix of a connected graph representing the communication between inverters.

The Laplacian of the communications graph is

$$G = \begin{bmatrix} g_{1,1} & -g_{1,2} & \cdots & -g_{1,n} \\ -g_{1,2} & g_{2,2} & \cdots & -g_{2,n} \\ \vdots & \vdots & \ddots & \vdots \\ -g_{1,n} & \cdots & -g_{n-1,n} & g_{n,n} \end{bmatrix} \tag{9}$$

where

$$g_{ii} \triangleq \sum_{j=1, j \neq i}^{n} g_{ij}. \tag{10}$$

Next, we incorporate the secondary control loop to the primary control by adding the integral state to the local frequency (4) with a small modification to filter the secondary control state as done in (5) for the active power. The proposed correction to (4) using the secondary controller is then

$$\omega_i = \omega^* - \eta_i (P_i^m - P_i^*) + \xi_i^m, \tag{11}$$

$$\tau_i \dot{\xi}_i^m = -\xi_i^m + \xi_i. \tag{12}$$

We obtain the dynamics of the closed-loop system that includes the primary and secondary control loops by combining (6)–(12)

$$\dot{\delta}_i = \omega_i, \tag{13}$$

$$\dot{\omega}_i = \tau_i^{-1} \Big(-(\omega_i - \omega_i^*) - \eta_i (P_i - P_i^*) + \xi_i \Big), \tag{14}$$

$$\dot{\xi}_i = k_i^{-1} \Big(-(\omega_i - \omega^*) - \sum_{j=1}^{n} g_{ij} (\xi_i - \xi_j) \Big). \tag{15}$$

We can also express the closed-loop system (13)-(15) in matrix form. We denote the vector $V = [v_i] \in \mathbb{R}^n$ as the column concatenation of scalars v_i, with $i = 1, \ldots, n$. Thus, we define $\Delta = [\delta_i]$, $\Omega = [\omega_i]$, $\Xi = [\xi_i]$, $P^* = [P_i^*]$, and $P_L = [P_{L,i}]$. And let $N \triangleq \text{diag}\{\eta_i\}$, $T \triangleq \text{diag}\{\tau_i\}$, and $K \triangleq \text{diag}\{k_i\}$. Then, the closed-loop dynamics is

$$\begin{bmatrix} \dot{\Delta} \\ T\dot{\Omega} \\ K\dot{\Xi} \end{bmatrix} = \begin{bmatrix} 0 & I & 0 \\ 0 & -I & I \\ 0 & -I & -G \end{bmatrix} \begin{bmatrix} \Delta \\ \Omega - \Omega^* \\ \Xi \end{bmatrix} + \begin{bmatrix} \Omega^* \\ NF(\Delta) + N(P^* - P_L) \\ 0 \end{bmatrix} \tag{16}$$

where vector $F(\Delta)$ has entries $-\sum_{j \in \mathcal{N}_i} \alpha_{ij} \sin(\delta_i - \delta_j)$. Note the trigonometric function comes from P_i in (14).

3) Synchronised Motion: As done in [4], we assume that there exist values for the angle differences, frequencies, and secondary control variables such that the closed loop (16) has a synchronised equilibrium motion.

Assumption 1: First, define the set

$$\mathcal{D} \triangleq \{\delta \in [0, 2\pi)^n \mid |\delta_i - \delta_j| < \pi/2, i \in \mathcal{N}, j \in \mathcal{N}_i\}. \tag{17}$$

For given values of $P_{L,i}$ and η_i, there exists constants $\delta^s \in \mathcal{D}$, $\omega^s \in \mathbb{R}$, and $\xi^s \in \mathbb{R}$, $i \in \mathcal{N}$, such that

$$1_n \omega^s = 1_n \omega^* + N(P - P^*) + 1_n \xi^s, \tag{18}$$

This article has been accepted for publication in IEEE Control Systems Letters. This is the author's version which has not been fully edited and content may change prior to final publication. Citation information: DOI 10.1109/LCSYS.2021.3114143

where 1_n is the vector of ones, and $P = [P_i] \in \mathbb{R}^n$.

Under Assumption 1, there exists a synchronised motion for the controlled system, with $\Omega = 1_n\omega^s$, $\Xi = 1_n\xi^s$, and $\Delta = \text{mod}_{2\pi}\{\delta^s + 1_n\omega^s t\}$, for $i \in \mathcal{N}$, where the operation $\text{mod}_{2\pi}(\cdot)$ is performed element-wise [13]. A special case of Lemma 1, presented later, shows that the desired frequency ω^* is an equilibrium of the system (16), as $\omega^s = w^*$.

The limitation we observed with this controller configuration is that the closed-loop dynamics (16), under some system characteristics, may suffer from string instability and the performance of the network degrades as the number of inverters n increases. In the next section, we present a definition of string stability and a control design that guarantees string stability properties for the inverter network.

III. Control Objectives and Design

Our objective is to design a frequency controller for the interconnected inverters that ensures string stability. To present the string stability property proposed by Besselink and Johansson in [14], we consider a network of n agents whose dynamics can be written in the general compact form

$$\dot{x}_i = f_i(x_i, x_{i-1}, x_{i+1}) + d_i(t) \tag{19}$$

where x_i is the state vector of the ith agent, the function f_i describe its dynamics, and $d_i \in \mathbb{R}^3$ is the disturbance vector.

Definition 1 (Disturbance String Stability): Consider the system (19) and assume that $x_i^\star$ is a solution to its unperturbed dynamics. Then, the equilibrium $x_i^\star$ is said to be *disturbance string stable* if there exists a $\mathcal{KL}$ function β and a $\mathcal{K}_\infty$ function γ such that, for any disturbance d_i and initial conditions the estimate

$$\begin{aligned}\sup_i |x_i(t) - x_i^\star(t)|_2 \leq \beta\left(\sup_i |x_i(0) - x_i^\star(0)|_2, t\right) \\ + \gamma\left(\sup_i \|d_i(t)\|_\infty\right)\end{aligned} \tag{20}$$

is verified $\forall t > 0$ and $n \in \mathbb{N}$. The functions $\beta(\cdot,\cdot)$ and $\gamma(\cdot)$ are independent of n, and thus the inequality of the state error norm is the same for all inverters, regardless of the number of inverters. Notice that (20) ensures asymptotic stability for the undisturbed case (see [15, Section 2.5]), which implies $x_i \to x_i^\star$ as $t \to \infty$.

A. Sufficient Conditions for DSS

For our control design, we will make use of the sufficient conditions for DSS of (19) proposed in [16], which are

C1 $f_i(x_i^\star, x_{i-1}^\star, x_{i+1}^\star) = 0$

C2 for some $c \neq 0$ and $b > 0$

$$\begin{aligned}&\mu_2\left(\frac{\partial f_i(x_i)}{\partial x_i}\right) \leq -c^2, \\ &\max\left\{\left\|\frac{\partial f_i(x_i)}{\partial x_{i-1}}\right\|_2, \left\|\frac{\partial f_i(x_i)}{\partial x_{i+1}}\right\|_2\right\} \leq b, \\ &\text{for all } x_i, x_{i-1}, x_{i+1} \in \mathbb{R}^3;\end{aligned} \tag{21}$$

C3 $2b < c^2$.

where $x_i^\star = [\delta_i^s + \omega^* t \ \omega^* \ \xi^*]^T$ is the equilibrium of the system, $\mu_2(A) = \max_i(\lambda_i[A]_s)$, $[A]_s$ is the symmetric part of A, and $\lambda(A)$ is the vector of eigenvalues of A.

If **C1**-**C3** are satisfied, then the system (19) is DSS with

$$\begin{aligned}\sup_i |x_i(t) - x_i^\star(t)|_2 \leq e^{-\bar{c}^2 t} \sup_i |x_i(0) - x_i^\star(0)|_2 \\ + \frac{1 - e^{-\bar{c}^2 t}}{\bar{c}^2} \sup_i \|d_i(t)\|_\infty\end{aligned} \tag{22}$$

where $\bar{c}^2 = c^2 - b(1 + \max_i \varepsilon_i)$.

As the dynamics of the networked inverters (13), (14), (15) can be written in the compact form (19), the conditions **C1**-**C3** are instrumental to select the control gains that ensure the string stability property of the closed-loop system. However, the search for these gains is sometimes difficult or the sufficient conditions cannot be satisfied. We observed this problem for examples of "chains" of inverters under the primary and secondary control loops discussed in Section II, and thus DSS could not be guaranteed.

B. DSS Inverter Networks

In this section, we present a control structure that enables us to ensure DSS of the inverter chain. We propose an alternative consensus algorithm for the secondary controller so that the closed-loop dynamics can be written as

$$\dot{\delta}_i = \omega_i, \tag{23}$$

$$\dot{\omega}_i = \tau_i^{-1}\Big(-(\omega_i - \omega^*) - \eta_i(P_i - P_i^*) + \xi_i\Big), \tag{24}$$

$$\dot{\xi}_i = k_i^{-1}\Big(-(\omega_i - \omega^*) - \sum_{j=1}^{n}\big(g_{ij}(\xi_i - \xi_j) + l_{ij}(\delta_i - \delta_j)\big)\Big). \tag{25}$$

where l_{ij} are the elements of a connected graph L, which represents the communication of the inverter voltage angles. The coefficients l_{ij} are selected to verify $L = \kappa G$ for some constant $\kappa \in \mathbb{R}$.

Notice that, compared to (8), the new protocol of the secondary control (25) incorporates a term that is proportional to the difference between the voltage angles of neighbour inverters.

The closed-loop dynamics can be written compactly as

$$\begin{bmatrix}\dot{\Delta}\\ \dot{\Omega}\\ \dot{\Xi}\end{bmatrix} = \begin{bmatrix}0 & I & 0\\ 0 & -T^{-1} & T^{-1}\\ -K^{-1}L & -K^{-1} & -K^{-1}G\end{bmatrix}\begin{bmatrix}\Delta\\ \Omega - \Omega^*\\ \Xi\end{bmatrix} + \begin{bmatrix}\Omega^*\\ T^{-1}N\tilde{F}(\Delta) + T^{-1}N(P^* - P_L)\\ 0\end{bmatrix} \tag{26}$$

where $\tilde{F}(\Delta)$ has entries $-\sum_{j\in\mathcal{N}_i}\alpha_{ij}\sin(\delta_i - \delta_j)$.

Lemma 1: Consider that Assumption 1 holds and $L = \kappa G$ for some constant $\kappa \in \mathbb{R}$, then the desired frequency ω^* is an equilibrium of the system (26) as $\omega^s = \omega^*$.

Proof: Consider the equilibrium point (Ω^s, Ξ^s). From the last row in (26), we have

$$\Omega^s - \Omega^* = \Omega^s - 1_n\omega^* = -L\Delta^s - G\Xi^s, \tag{27}$$

$$1_n(\omega^s - \omega^*) = -G(\kappa\Delta^s - \Xi^s), \tag{28}$$

This article has been accepted for publication in IEEE Control Systems Letters. This is the author's version which has not been fully edited and content may change prior to final publication. Citation information: DOI 10.1109/LCSYS.2021.3114143

where $\kappa = \frac{l_{ii}}{g_{ii}}$. To obtain (28), we used the fact that $L = \kappa G$.

First, we notice from (9) that the vector 1_n is in the nullspace of the matrix G, that is $G1_n = 0$. Hence the column space of G does not contain the vector 1_n. Thus, if a synchronised solution exists $\Omega^s = 1_n\omega^s$, it must be equal to the set-point, that is $1_n\omega^s = 1_n\omega^*$ and $\omega_i^s = \omega^*$, $i \in \mathcal{N}$, which concludes the proof. ■

We present the following theorem, which follows the idea in [17], to show that the changes in the structure of the secondary controller (25) allow us to guarantee string stability of the closed-loop system (26).

Theorem 1: Consider the proposed secondary controller and the resulting closed-loop dynamics (23)-(25), such that the following conditions are satisfied:

C1* $f_i(x_i^\star, x_{i-1}^\star, x_{i+1}^\star) = 0$

C2* for some $c \neq 0$ and $b > 0$

$$\begin{aligned} &\mu_2\left(J_{i,i}\right) \leq -c^2, \\ &\max\left\{\left\|J_{i,i-1}\right\|_2, \left\|J_{i,i+1}\right\|_2\right\} \leq b, \\ &\text{for all } x_i, x_{i-1}, x_{i+1} \in \mathbb{R}^3; \end{aligned} \tag{29}$$

where $J_{i,i} = \Gamma \dfrac{\partial f_i(x_i)}{\partial x_i}\Gamma^{-1}$, and $J_{i,i\pm1} = \Gamma \dfrac{\partial f_i(x_i)}{\partial x_{i\pm1}}\Gamma^{-1}$

C3* $2b < c^2$.

where $\Gamma \in \mathbb{R}^{3\times3}$ is a constant matrix to be selected. Then, the closed loop (23)-(25) is DSS.

Proof: Consider the state transformation $z_i = \Gamma x_i$. Then, the transformed dynamics can be written as

$$\dot{z}_i = \Gamma\, f_i(\Gamma^{-1}z_i, \Gamma^{-1}z_{i-1}, \Gamma^{-1}z_{i+1}, \Gamma^{-1}z_n) + \Gamma d_i. \tag{30}$$

If conditions **C1*-C3*** are satisfied, the transformed system is DSS and the states are bounded as follows

$$\begin{aligned} \sup_i \left|z_i(t) - z_i^\star(t)\right|_2 \leq\ & e^{-\bar{c}^2 t} \sup_i \left|z_i(0) - z_i^\star(0)\right|_2 \\ &+ \frac{1 - e^{-\bar{c}^2 t}}{\bar{c}^2} \sup_i \left\|\tilde{d}_i(t)\right\|_\infty, \end{aligned} \tag{31}$$

where $\tilde{d}_i = \Gamma d_i$.

Substituting $x_i = \Gamma^{-1}z_i$ in (31) and using the minimum and maximum singular value of Γ, we obtain

$$\begin{aligned} \sup_i \left|x_i(t) - x_i^\star(t)\right|_2 \leq\ & K e^{-\bar{c}^2 t} \sup_i \left|x_i(0) - x_i^\star(0)\right|_2 \\ &+ K\frac{1 - e^{-\bar{c}^2 t}}{\bar{c}^2} \sup_i \left\|d_i(t)\right\|_\infty, \end{aligned} \tag{32}$$

where $K = \frac{\max_i(\sigma_{\max}(\Gamma))}{\min_i(\sigma_{\min}(\Gamma))}$, and $\sigma_{\min}(\Gamma)$ and $\sigma_{\max}(\Gamma)$ denote the minimum and maximum singular value of Γ. From the DSS inequality (32), we conclude that the closed-loop system with the proposed controller is DSS. ■

The transformation matrix Γ adds an extra degree of freedom to find the controller gains that satisfy the DSS conditions. Without the transformation, we were not able to find gains that satisfy **C1-C3** for the closed loop dynamics in (26), in the original coordinates.

TABLE I
CONTROLLER GAIN VALUES.

Gain	DSS Controller C_1	Standard Controller C_2
τ_i	1.4895	1
η_i	6.3509×10^{-4}	3×10^{-3}
k_i	4.9481	1
$g_{i,i\pm1}$	0.0213	1
$l_{i,i\pm1}$	0.0043	0

TABLE II
NETWORK PARAMETERS AND INVERTERS INITIAL CONDITION.

Parameter	Values
V	325.3 V
ω^*	50 Hz
b_{ij}	$\{-0.0056, -0.0112, -0.0039, -0.0112\}$
P_i^*	1260 W
$P_{L,i}$	1260 W
$\delta_i(0)$	0
$\omega_i(0)$	50 Hz
$\xi_i(0)$	0

IV. SIMULATION RESULTS AND DISCUSSION

In this section, we present simulations of the closed-loop system (26), which is obtained by using the DSS controller proposed in this paper and denoted as C_1. We compare the results against the closed-loop system (16), denoted C_2, which uses a standard controller (e.g. [11]).

A. Simulations

We simulated "chains" of $n = 4$ to $n = 20$ inverters connected using a communication graph in a ring topology (*i.e.* the last inverter is connected to the first). The gains for the controllers are reported in Table I and the model parameters and initial conditions are shown in Table II.

The system set-up is similar to that in [11], but the active power demands of the loads connected to all inverters is $P_L = 1260$ W. At $t = 0$ s, the load connected to the inverter $i = 1$ is increased by 20% and the loads connected to every even inverter $i = \{2, 4, \ldots, n\}$ are increased by 10%. The loads are changed back to their rated values at $t = 1500$ s. We simulated chains of inverters starting with 4 inverters and adding 2 inverters each time up to a chain of 20 inverters. The additional susceptance b_{ij} between the added inverters is randomly picked from the values in Table II.

The L_∞ norm of the state error ($\sup_t \left|x_i(t) - x_i^\star(t)\right|_2$) for the inverters is shown in Fig. 1. It can be seen that the state error norm remains bounded when using the DSS controller C_1 as expected. On the other hand, the norm increases when the number of inverters increases when using the controller C_2, which suggests that string instability could happen in such a closed-loop system. Fig. 2 and 3 show the L_∞-norms of the active and reactive power injections, $\sup_t \left|P_{I,i}\right|_2$ (see (2)) and $\sup_t \left|Q_i\right|_2$, where $Q_i = |B_{ii}|V_i^2 - \sum_{j\in\mathcal{N}_i} |B_{ij}|V_iV_j\cos(\delta_i - \delta_j)$. Note that the power injections are bounded for C_1 whilst, for C_2, the power injections increase about 25% when the number of inverters increases from 4 to 20, while the reactive power increases about 300% under the same scenario.

This article has been accepted for publication in IEEE Control Systems Letters. This is the author's version which has not been fully edited and content may change prior to final publication. Citation information: DOI 10.1109/LCSYS.2021.3114143

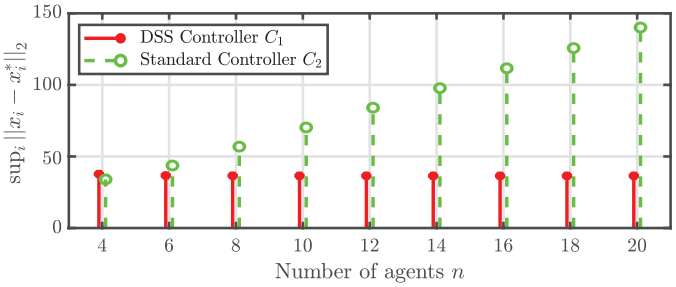

Fig. 1. L_∞ state error norm of the simulated inverter chains using the DSS controller (red) and the standard controller (green).

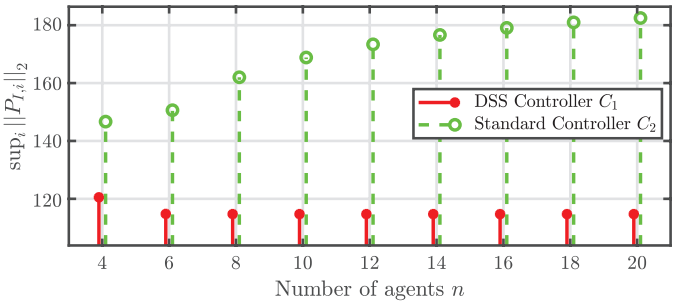

Fig. 2. L_∞ norm of power injections $P_{I,i}$, as in (2), of the chains using the DSS controller (red) and the standard controller (green).

We also present the time history of some relevant variables for the chains of 4 and 12 inverters. Figs. 4 and 5 show, respectively, the frequency and active power at every inverter node for a "chain" of 4 inverters, using the DSS controller. Similarly, Figs. 6 and 7 show the frequency and active power when the standard controller is used. The frequency and active power for the chain of 12 inverters using the DSS controller and the standard controller are shown in Figs. 8 to 11.

We notice that the growth of state error norm is related to an increment in the deviation of voltage angles δ_i from the desired voltage angle $\delta^* = \delta^s + \omega^* t$, which in turn reflects in the L_∞-norm of the active power injections, shown in Fig. 2. This motivated the inclusion of voltage angle communication between neighbour inverters in the DSS controller design. Also, the standard controller provides a better power sharing performance, with the inverters injecting/receiving power symmetrically, and with groups of inverters with the same

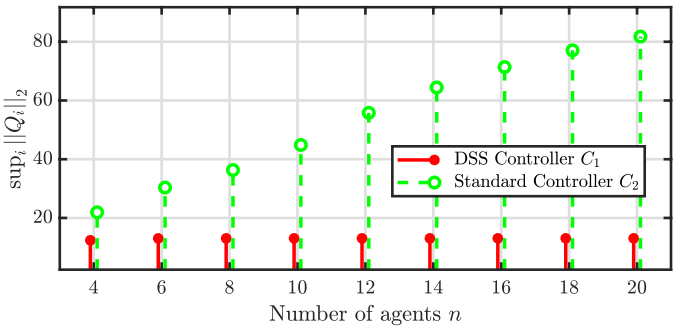

Fig. 3. L_∞ norm of the reactive power Q_i for the simulated inverter chains using the DSS controller (red) and the standard controller (green).

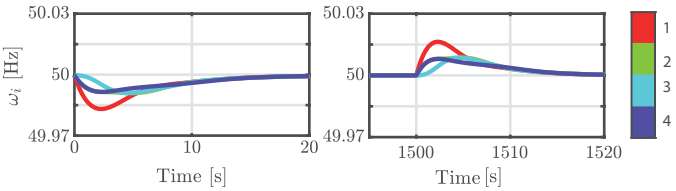

Fig. 4. Time history of the frequency for a chain of 4 inverters using the DSS controller.

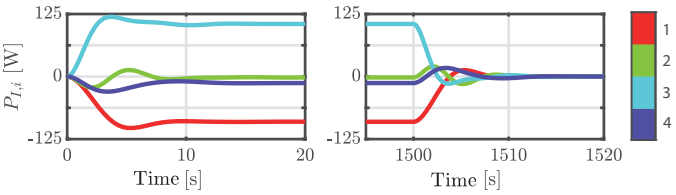

Fig. 5. Time history of the active power injections $P_{I,i}$ as in (2) for a chain of 4 inverters using the DSS Controller.

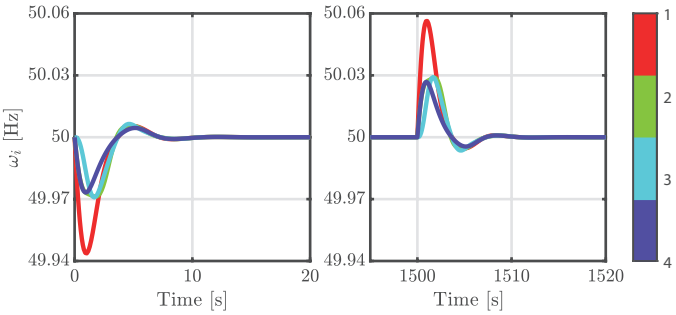

Fig. 6. Time history of the frequency for a chain of 4 inverters using the standard controller.

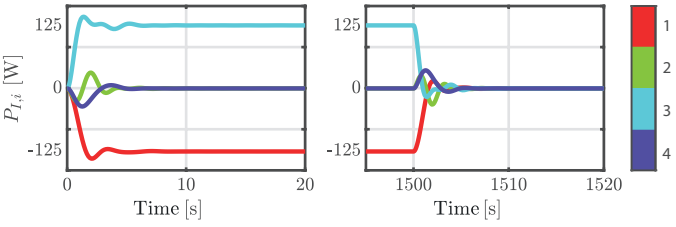

Fig. 7. Time history of the active power injections $P_{I,i}$ as in (2) for a chain of 4 inverters using the standard Controller.

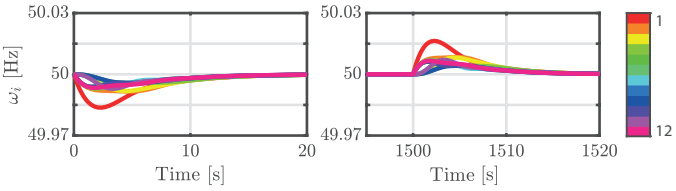

Fig. 8. Time history of the frequency for a chain of 12 inverters using the DSS controller.

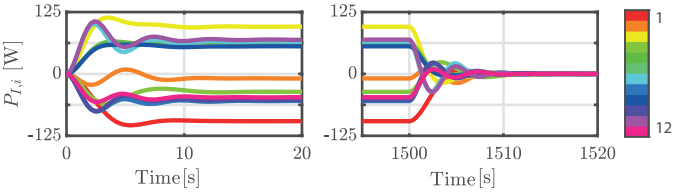

Fig. 9. Time history of the active power injections $P_{I,i}$ as in (2) for a chain of 12 inverters using the DSS Controller.

This article has been accepted for publication in IEEE Control Systems Letters. This is the author's version which has not been fully edited and content may change prior to final publication. Citation information: DOI 10.1109/LCSYS.2021.3114143

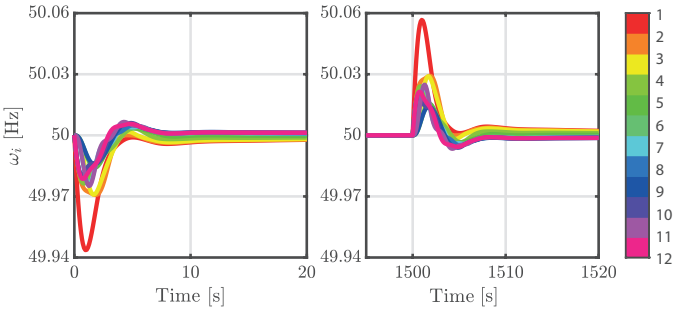

Fig. 10. Time history of the frequency for a chain of 12 inverters using the standard controller.

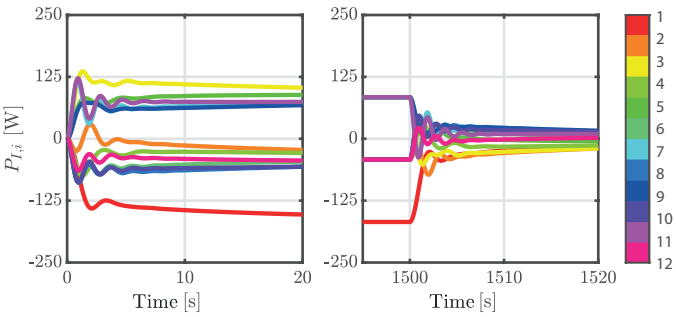

Fig. 11. Time history of the active power injections $\boldsymbol{P_{I,i}}$ as in (2) for a chain of 12 inverters using the standard Controller.

disturbance converging to the same value (see Fig. 7), but the infinite norms of the active power injection and reactive power are larger when the number of inverters increases (see Fig. 2). The closed loop with the standard controller is stable for any choice of positive gains. However, we observed that if the gains are not selected carefully, the system may suffer from string instability, preventing its scalability. The proposed DSS controller ensures that the state errors do not grow unbounded with the increment of inverters in the chain while maintaining satisfactory performance.

V. Conclusion

We identified the problem of string instability in inverter-based microgrids and presented a controller design that guarantees DSS of the frequency control in chains of inverters. In this work, we considered that the inverters' voltage is constant. In future works, we will consider the voltage control loop and investigate the scalability properties of the control system. Finally, although the presentation was based on radial microgrids, the proposed controller design to guarantee DSS can be readily extended, with the appropriate modifications, to microgrids of arbitrary topology.

Acknowledgements

G.F.S., A.M., and J.F. acknowledge continued support from the Queensland University of Technology (QUT) through the Centre for Robotics. This work was supported in part by the Australian Research Council through grant DP190102859. We thank Assist. Prof. J. W. Simpson-Porco, Dr. S. Stüdli, and Prof. D. Quevedo for fruitful discussions.

References

[1] J. M. Guerrero, J. C. Vasquez, J. Matas, L. G. de Vicuña, and M. Castilla, "Hierarchical control of droop-controlled AC and DC microgrids—A general approach toward standardization," *IEEE Transactions on Industrial Electronics*, vol. 58, no. 1, pp. 158–172, 2011.

[2] A. Bidram, A. Davoudi, F. L. Lewis, and J. M. Guerrero, "Distributed cooperative secondary control of microgrids using feedback linearization," *IEEE Transactions on Power Systems*, vol. 28, no. 3, pp. 3462–3470, 2013.

[3] Q. Shafiee, J. M. Guerrero, and J. C. Vasquez, "Distributed secondary control for islanded microgrids—A novel approach," *IEEE Transactions on Power Electronics*, vol. 29, no. 2, pp. 1018–1031, 2014.

[4] J. Schiffer, R. Ortega, A. Astolfi, J. Raisch, and T. Sezi, "Conditions for stability of droop-controlled inverter-based microgrids," *Automatica*, vol. 50, no. 10, pp. 2457–2469, 2014.

[5] R. Heidari, M. M. Seron, and J. H. Braslavsky, "Ultimate boundedness and regions of attraction of frequency droop controlled microgrids with secondary control loops," *Automatica*, vol. 81, pp. 416 – 428, 2017.

[6] C. De Persis, N. Monshizadeh, J. Schiffer, and F. Dörfler, "A Lyapunov approach to control of microgrids with a network-preserved differential-algebraic model," in *IEEE Conference on Decision and Control*, 2016, pp. 2595–2600.

[7] A. Silani, M. Cucuzzella, J. M. A. Scherpen, and M. J. Yazdanpanah, "Output regulation for load frequency control," *IEEE Transactions on Control Systems Technology*, pp. 1–15, 2021.

[8] A. Bidram, F. L. Lewis, and A. Davoudi, "Distributed control systems for small-scale power networks: Using multiagent cooperative control theory," *IEEE Control Systems Magazine*, vol. 34, no. 6, pp. 56–77, 2014.

[9] P. Kundur, *Power System Stability And Control*, ser. EPRI power system engineering series. McGraw-Hill, 1994.

[10] F. Dörfler, J. W. Simpson-Porco, and F. Bullo, "Breaking the hierarchy: Distributed control and economic optimality in Microgrids," *IEEE Transactions on Control of Network Systems*, vol. 3, no. 3, pp. 241–253, 2016.

[11] J. W. Simpson-Porco, Q. Shafiee, F. Dörfler, J. C. Vasquez, J. M. Guerrero, and F. Bullo, "Secondary frequency and voltage control of islanded microgrids via distributed averaging," *IEEE Transactions on Industrial Electronics*, vol. 62, no. 11, pp. 7025–7038, 2015.

[12] J. Schiffer, D. Goldin, J. Raisch, and T. Sezi, "Synchronization of droop-controlled microgrids with distributed rotational and electronic generation," in *IEEE Conference on Decision and Control*, 2013, pp. 2334–2339.

[13] J. W. Simpson-Porco, F. Dörfler, and F. Bullo, "Synchronization and power sharing for droop-controlled inverters in islanded microgrids," *Automatica*, vol. 49, no. 9, pp. 2603–2611, 2013.

[14] B. Besselink and K. H. Johansson, "String stability and a delay-based spacing policy for vehicle platoons subject to disturbances," *IEEE Transactions on Automatic Control*, vol. 62, no. 9, pp. 4376–4391, 2017.

[15] E. D. Sontag, *Input to State Stability: Basic Concepts and Results*. Berlin, Heidelberg: Springer Berlin Heidelberg, 2008, pp. 163–220.

[16] J. Monteil, G. Russo, and R. Shorten, "On $\mathcal{L}_\infty$ string stability of nonlinear bidirectional asymmetric heterogeneous platoon systems," *Automatica*, vol. 105, pp. 198–205, Jul. 2019.

[17] G. F. Silva, A. Donaire, A. McFadyen, and J. J. Ford, "String stable integral control design for vehicle platoons with disturbances," *Automatica*, vol. 127, p. 109542, 2021.